Product of the SNPP VIIRS SD screen transmittance and the SD BRDF (RSB) from both yaw maneuver and regular on-orbit data

Ning Lei[1, *] and Xiaoxiong Xiong[2]

1. Science Systems and Applications, Inc., 10210 Greenbelt Road, Suite 600, Lanham, MD 20706 USA; ning.lei@ssaihq.com
2. Sciences and Exploration Directorate, NASA Goddard Space Flight Center, Greenbelt, MD, MD 20771 USA; xiaoxiong.xiong-1@nasa.gov

*** Author to whom correspondence should be addressed:** Tel: +1-301-867-2066

ABSTRACT

To assure data quality, the Earth-observing Visible Infrared Imaging Radiometer Suite (VIIRS) regularly performs on-orbit radiometric calibrations of its 22 spectral bands. The primary calibration radiance source for the reflective solar bands (RSBs) is a sunlit solar diffuser (SD). During the calibration process, sunlight goes through a perforated plate (the SD screen) and then strikes the SD. The SD scattered sunlight is used for the calibration, with the spectral radiance proportional to the product of the SD screen transmittance and the SD bidirectional reflectance distribution function (BRDF). The BRDF is decomposed to the product of its value at launch and a numerical factor quantifying its change since launch. Therefore, the RSB calibration requires accurate knowledge of the product of the SD screen transmittance and the BRDF (RSB; launch time). Previously, we calculated the product with yaw maneuver data and found that the product had improved accuracy over the prelaunch one. With both yaw maneuver and regular on orbit data, we were able to improve the accuracy of the SDSM screen transmittance and the product for the solar diffuser stability monitor SD view. In this study, we use both yaw maneuver and a small portion of regular on-orbit data to determine the product for the RSB SD view.

Index Terms: SNPP VIIRS, radiometric calibration, RSB, solar diffuser, BRDF degradation, solar diffuser screen transmittance, yaw maneuver

1. INTRODUCTION

To continue providing satellite data to study the Earth, the Suomi National Polar-orbiting Partnership (SNPP) satellite was launched on October 28, 2011, carrying five scientific instruments. One of the instruments is the Visible Infrared

Imaging Radiometer Suite (VIIRS), with fourteen reflective solar bands (RSBs), seven thermal emissive bands, and one Day-Night band. With a hardware design based on heritage satellite sensors such as the still-operational Moderate Resolution Imaging Spectroradiometer (MODIS) on Terra and Aqua satellites[1-2], the VIIRS instrument is a passive scanning radiometer, able to cover the entire earth surface every two days[3-4]. To ensure data quality, the VIIRS regularly performs on-orbit radiometric calibrations[5-6].

On-orbit radiometric calibration is meant to allow for accurate determination of the estimated top-of-the-atmosphere hemispherical spectral reflectance[7]. Primarily using an onboard sunlit solar diffuser (SD) panel, the VIIRS performs on-orbit radiometric calibration of the RSBs. Sunlight goes through the holes on a perforated plate (the SD screen) and then strikes the SD surface. The SD surface diffusely scatters the incident sunlight in a near-Lambertian way to provide a radiance source to calibrate the RSBs. The spectral radiance of the scattered sunlight is proportional to the product of the SD screen transmittance and the SD bidirectional reflectance distribution function (BRDF). The BRDF value decreases over time, probably due to exposure to solar radiative energy and high energy particles, and perhaps on-orbit contamination [8-9]. A numerical factor, denoted as the BRDF degradation factor, is conventionally used to quantify the decrease[7, 10]. Mathematically we write the spectral radiance of the SD scattered sunlight as

$$L \propto \tau_{\mathrm{SD}}\left(\vec{\phi}\right)\mathrm{BRDF}\left(\lambda, t=0; \vec{\phi}(t), \vec{\phi}_{\mathrm{RTA}}\right) \times H\left(\lambda, t; \vec{\phi}(t), \vec{\phi}_{\mathrm{RTA}}\right) \quad . \tag{1}$$

In Eq. (1), $\vec{\phi}$ represents the solar angle relative to the SD surface and $\vec{\phi}_{\mathrm{RTA}}$ represents the angle of the scattered light relative to the SD that goes to the RSB focal planes through the rotating telescope assembly (RTA). Thus, we need to know the product of the SD screen transmittance and the BRDF at the RTA SD view direction at time zero: $\tau_{\mathrm{SD}}\left(\vec{\phi}\right)\mathrm{BRDF}\left(\lambda, t=0; \vec{\phi}, \vec{\phi}_{\mathrm{RTA}}\right)$. To simplify our notation, we denote $\tau_{\mathrm{SD}}\left(\vec{\phi}\right)\mathrm{BRDF}\left(\lambda, t=0; \vec{\phi}, \vec{\phi}_{\mathrm{RTA}}\right)$ as $\tau_{\mathrm{SD}}\,\mathrm{BRDF}_{\mathrm{RTA}}$.

The SD screen transmittance and the SD BRDF were measured prelaunch. Based on the experience from the MODIS instruments[11], to improve the accuracies of the screen transmittances, including the SDSM screen, satellite yaw maneuvers were carried out around 110 days after the satellite launch. Note that the absolute value of $\tau_{\mathrm{SD}}\,\mathrm{BRDF}_{\mathrm{RTA}}$ may not be determined directly from the yaw maneuver data and we may need the prelaunch $\tau_{\mathrm{SD}}\,\mathrm{BRDF}_{\mathrm{RTA}}$ to determine the absolute value. In previous publications, we showed that the solar azimuth angle step size in the yaw maneuvers is too large, shown in Fig. 1, resulting in large errors in the calculated SDSM screen relative transmittance[12-13] and noticeable errors in the calculated relative product $\tau_{\mathrm{SD}}\,\mathrm{BRDF}_{\mathrm{SDSM}}$ [14]. We improved the accuracies of the SDSM screen relative transmittance and the relative $\tau_{\mathrm{SD}}\,\mathrm{BRDF}_{\mathrm{SDSM}}$ with both yaw maneuver and a small portion of regular on-orbit data. Similarly, in this study, to improve the accuracy of $\tau_{\mathrm{SD}}\,\mathrm{BRDF}_{\mathrm{RTA}}$ calculated from the yaw maneuver data, we use a small portion of regular on-orbit data.

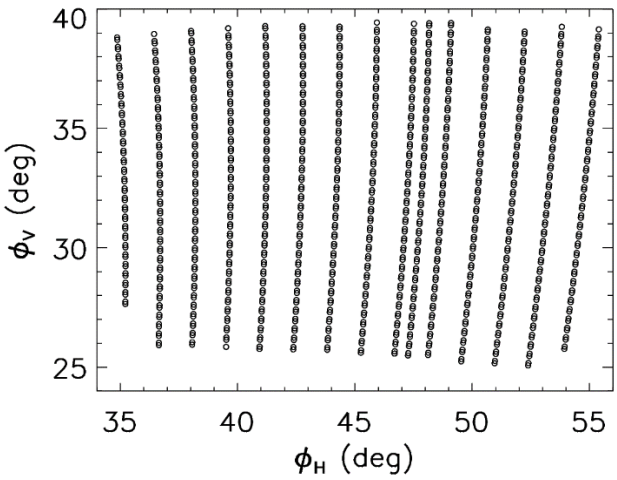

Fig. 1. Solar angles in the SD coordinate system (see Section 2 for the definition) when the RTA views the sunlit SD during the yaw maneuvers and the dual-gain bands are in the high-gain stage.

2. SD BRDF DEGRADATION FACTOR ANGULAR DEPENDENCE IN THE RTA SD VIEW DIRECTION

In Ref. 15, we calculated $\tau_{SD}\,\mathrm{BRDF}_{RTA}$ from the yaw maneuver data alone. To remove the bias in the previously calculated $\tau_{SD}\,\mathrm{BRDF}_{RTA}$ [16], we applied the angular dependence of the BRDF degradation factor. As an example, the ϕ_V dependence of the degradation factor for the RTA SD view is plotted in Fig. 2, where ϕ_V is the angle between the solar light and the SD surface. The figure shows the dependence determined by the SD observation data from the M1-M7 bands at satellite orbits 5447 and 10838; the data from other RSBs are much nosier. Those satellite orbits correspond to

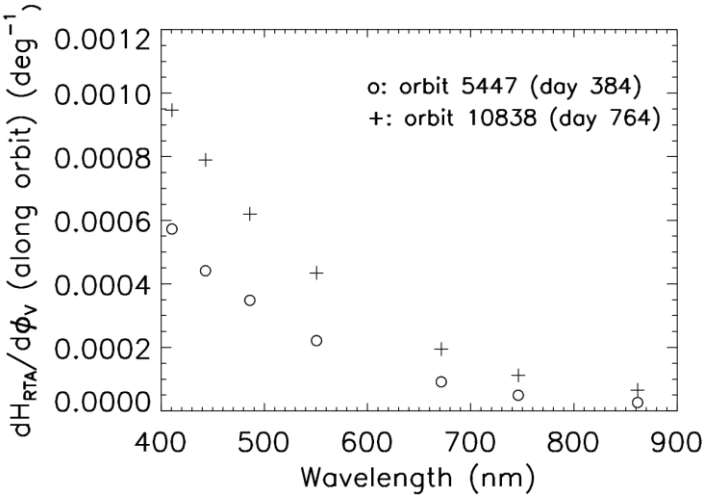

Fig. 2. $\partial H_{RTA}/\partial\phi_V$ along the satellite orbits 5447 (circles) and 10838 (pluses), respectively. The dependence is calculated with the SD observation data from the M1-M7 bands.

days 384 and 764, respectively, after the satellite launch. The standard deviations of the errors of the determined dependences are around low 10^{-5} per degree which is small, allowing for accurate bias removal in the calculated

$\tau_{SD}\,\mathrm{BRDF}_{RTA}$ with the largest bias in the low 10^{-4}. The ϕ_V dependence of the degradation factor for the RTA SD view may be approximated by[15, 17]

$$\frac{\partial H_{RTA}}{\partial \phi_V}(\text{along orbit}) = 0.0042 \times (1 - H_{SDSM}(\phi_V = 35.5°)) - 0.0038 \times (1 - H_{SDSM}(\phi_V = 35.5°))^2 . \quad (2)$$

In Eq. (2), H_{SDSM} is the BRDF degradation factor along the SDSM SD view direction.

The dependence on the azimuth angle is determined from the yearly sensor gain undulation with respect to the angle, with the gain computed using the H_{SDSM} [17]. H_{SDSM} is insensitive to the variation of the azimuth angle since the SDSM views the SD nearly perpendicularly, as shown schematically in Fig. 3.

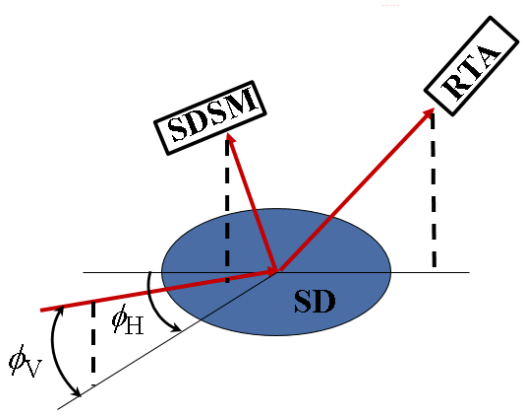

Fig. 3. Solar angles in the SD coordinate system. The x-axis is the SD-to-RTA view vector projected onto the SD surface and the z-axis is the SD surface normal vector. The y-axis is formed from the right-hand rule.

3. DETERMINATION OF $\tau_{SD}\,\mathrm{BRDF}_{RTA}$ FROM BOTH YAW MANEUVER AND A SMALL PORTION OF REGULAR ON-ORBIT DATA

The small portion of regular on-orbit data used, shown in Fig. 4, is from nearly the same orbits as those for the determination of the SDSM screen transmittance[12-13] and the relative product of the SD screen transmittance and the BRDF at the satellite launch time (t=0) for the SDSM SD view[14]. To significantly reduce the adverse impact of the nonlinear drifts of the detector gain and solar power, we divide the regular on-orbit data into smaller segments. Each segment covers the solar angles of one yaw maneuver orbit. To cover the solar angles with exceptionally small ϕ_H (large ϕ_H in the VIIRS coordinate system) occurring around orbit 15700, we add an additional data segment centered on orbit 15264. Additionally, we replace the data segment centered on orbit 4541 with a data segment centered on orbit 6271 to improve data quality. Fig. 4 also shows a small portion of regular on-orbit data that we use for validation.

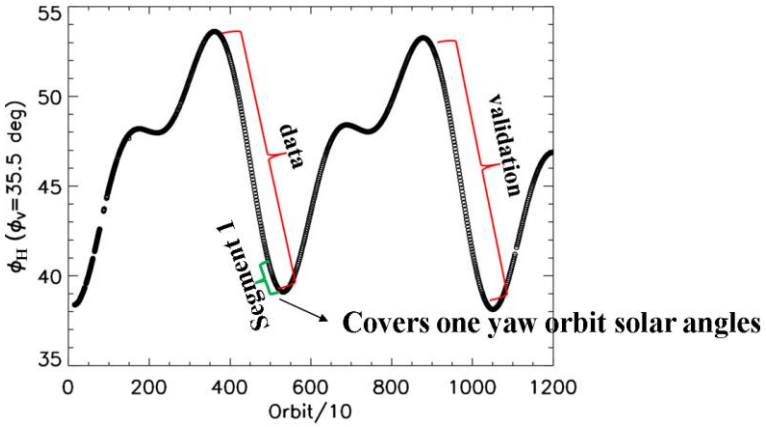

Fig. 4. Solar azimuth angle in the SD coordinate system vs. satellite orbit numbers when the RTA views the sunlit SD at $\phi_V = 35.5°$.

We determine the relative product of the SD screen transmittance and the BRDF at t=0 through the following

$$\frac{\tau_{SD}\left(\vec{\phi}(t),\, d,\, B\right)\mathrm{BRDF}_{\,RTA}\left(\lambda_B,\, t=0,\, \vec{\phi}(t)\right)}{\tau_{SD}\left(\vec{\phi}(t_{mid}),\, d,\, B\right)\mathrm{BRDF}_{\,RTA}\left(\lambda_B,\, t=0,\, \vec{\phi}(t_{mid})\right)} = \frac{F(t)*\left(c_0 + dn_{SD}(t) + c_2 dn_{SD}^2(t)\right)}{F(t_{mid})*\left(c_0 + dn_{SD}(t_{mid}) + c_2 dn_{SD}^2(t_{mid})\right)} \times \frac{\cos\theta_{SD\text{-}sun}(t_{mid})}{\cos\theta_{SD\text{-}sun}(t)} \times \frac{\int d\lambda * \mathrm{RSR}_{\,RSB}(\lambda,\, t_{mid},\, B) E_{sun}(\lambda, t_{mid}) H_{RTA}\left(\lambda, t_{mid}, \vec{\phi}(t_{mid})\right)}{\int d\lambda * \mathrm{RSR}_{\,RSB}(\lambda, t, B) E_{sun}(\lambda, t) H_{RTA}\left(\lambda, t, \vec{\phi}(t)\right)} \quad . \tag{3}$$

In Eq. (3), t_{mid} is a time in the middle of a data segment, $F(t)$ is a calibration correction factor to account for detector gain change, $E_{sun}(\lambda, t)$ is the solar spectral irradiance at the VIIRS position, $\mathrm{RSR}_{\,RSB}$ is the relative spectral response function for a detector in the RSBs, and $\theta_{SD\text{-}sun}$ is the angle between the solar vector and the SD surface normal. To reach Eq. (3), we used the property that the BRDF at t=0 is weakly dependent of the photon wavelength. Since a data segment is short in time, $F(t)$ and $E_{sun}(\lambda, t)$ can both be approximated by linear Taylor polynomials. We denote the linear term coefficients as c_F and c_E, for $F(t)$ and $E_{sun}(\lambda, t)$, respectively. Assuming that c_E is not strongly dependent on the photon wavelength within the $\mathrm{RSR}_{\,RSB}$ peak width, we re-write Eq. (3) as

$$\frac{\tau_{SD}\left(\vec{\phi}(t),\, d,\, B\right)\mathrm{BRDF}_{\,RTA}\left(\lambda_B,\, t=0,\, \vec{\phi}(t)\right)}{\tau_{SD}\left(\vec{\phi}(t_{mid}),\, d,\, B\right)\mathrm{BRDF}_{\,RTA}\left(\lambda_B,\, t=0,\, \vec{\phi}(t_{mid})\right)} = \frac{\left[1 + (c_F - c_E)\times(t - t_{mid})\right]*\left(c_0 + dn_{SD}(t) + c_2 dn_{SD}^2(t)\right)}{c_0 + dn_{SD}(t_{mid}) + c_2 dn_{SD}^2(t_{mid})} \times \frac{\cos\theta_{SD\text{-}sun}(t_{mid})}{\cos\theta_{SD\text{-}sun}(t)} \times \frac{\int d\lambda * \mathrm{RSR}_{\,RSB}(\lambda,\, t_{mid},\, B) E_{sun}(\lambda, t_{mid}) H_{RTA}\left(\lambda, t_{mid}, \vec{\phi}(t_{mid})\right)}{\int d\lambda * \mathrm{RSR}_{\,RSB}(\lambda, t, B) E_{sun}(\lambda, t_{mid}) H_{RTA}\left(\lambda, t, \vec{\phi}(t)\right)} \quad . \tag{4}$$

For simplicity, we denote the left hand side of Eq. (4) as $\tau_{\mathrm{SD}}^{\mathrm{R}}\,\mathrm{BRDF}_{\mathrm{RTA}}$. The initial value of $c_{\mathrm{F}} - c_{\mathrm{E}}$ comes from $F(t)$ calculated previously. For yaw maneuver data, $|t - t_{\mathrm{mid}}| <$ 0.5 day which is a very short time duration so that errors in $c_{\mathrm{F}} - c_{\mathrm{E}}$ do not contribute much in the calculated $\tau_{\mathrm{SD}}^{\mathrm{R}}\,\mathrm{BRDF}_{\mathrm{RTA}}$. We determine $\tau_{\mathrm{SD}}^{\mathrm{R}}\,\mathrm{BRDF}_{\mathrm{RTA}}$ from the yaw maneuver data first and then calculate $\tau_{\mathrm{SD}}^{\mathrm{R}}\,\mathrm{BRDF}_{\mathrm{RTA}}$ for each regular on-orbit data segment. For the $\tau_{\mathrm{SD}}^{\mathrm{R}}\,\mathrm{BRDF}_{\mathrm{RTA}}$ from a regular on-orbit data segment, we scale the $\tau_{\mathrm{SD}}^{\mathrm{R}}\,\mathrm{BRDF}_{\mathrm{RTA}}$ to match the $\tau_{\mathrm{SD}}^{\mathrm{R}}\,\mathrm{BRDF}_{\mathrm{RTA}}$ from the yaw maneuvers through a least-squares process. We then determine the error in $c_{\mathrm{F}} - c_{\mathrm{E}}$ through boundary value match and make a correction to the initial $c_{\mathrm{F}} - c_{\mathrm{E}}$. The boundary match means that for data points located in two neighboring regular on-orbit data segments, the relative product $\tau_{\mathrm{SD}}^{\mathrm{R}}\,\mathrm{BRDF}_{\mathrm{RTA}}$ should be the same and the difference is due to an error in the initial $c_{\mathrm{F}} - c_{\mathrm{E}}$. As an example, Fig. 5 shows the solar angles in two neighboring data segments.

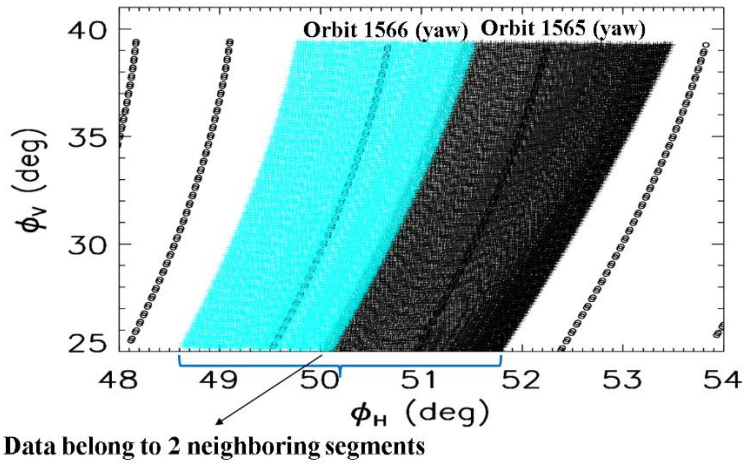

Fig. 5. Solar angles in the SD coordinate system for two neighboring data segments. The solar angles are shown when the RTA views the sunlit SD and the dual-gain bands are in the high-gain stage. The circles indicate the solar angles at a few yaw maneuver orbits.

After the steps described in the last paragraph, the match for $\tau_{\mathrm{SD}}^{\mathrm{R}}\,\mathrm{BRDF}_{\mathrm{RTA}}$ between the yaw maneuver and the regular on-orbit data is very good. The standard deviations of the differences averaged over the detectors in a band are 0.0013, 0.0013, 0.0023, 0.00060, 0.00048, 0.00036, 0.00030, 0.00033, 0.00032, 0.00028, 0.00094, 0.0012, 0.00084, 0.0013, for the I1-I3 and M1-M11 bands, respectively. Fig. 6 shows the match for the 8th detector of the M1 and M7 bands, in the high-gain stage, over solar angles on yaw maneuver orbit 1573 when the RTA views the sunlit SD.

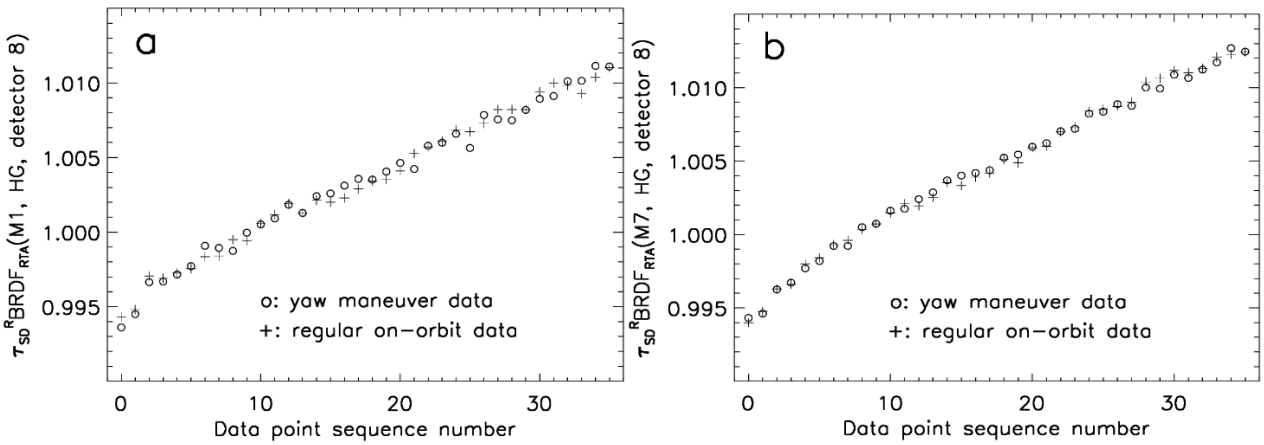

Fig. 6. The calculated $\tau_{SD}^{R}\,\mathrm{BRDF}_{\mathrm{RTA}}$ for detector 8 of bands (a) M1 and (b) M7, using high-gain data and with both the yaw maneuver data (circles) and a small portion of regular on-orbit data (pluses). The yaw maneuver data are from satellite orbit 1573. The pluses are the $\tau_{SD}^{R}\,\mathrm{BRDF}_{\mathrm{RTA}}$ from the regular orbit data segment centered on orbit 4917, interpolated at the yaw maneuver solar angles. The x axis is for the data point sequence number in the yaw maneuver data on orbit 1573.

We combine the $\tau_{SD}^{R}\,\mathrm{BRDF}_{\mathrm{RTA}}$ from both the yaw maneuver and regular on-orbit data. Considering the impact of random noise on the calculated $\tau_{SD}^{R}\,\mathrm{BRDF}_{\mathrm{RTA}}$, we use the $\tau_{SD}^{R}\,\mathrm{BRDF}_{\mathrm{RTA}}$ from the yaw maneuver data over the solar angles

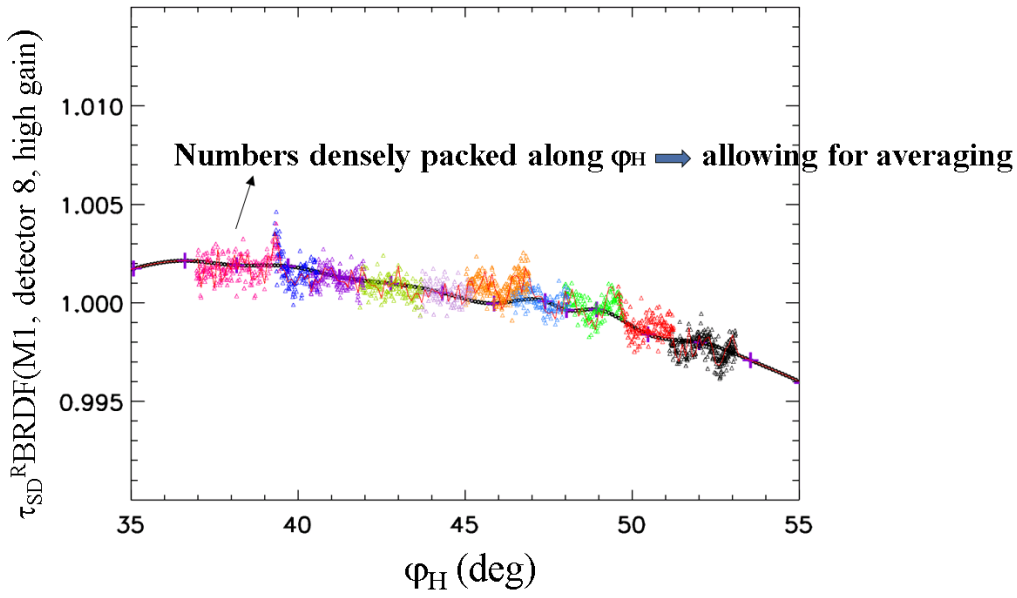

Fig. 7. The calculated $\tau_{SD}^{R}\,\mathrm{BRDF}_{\mathrm{RTA}}$ for detector 8 of band M1 in the high-gain stage at φv=35.5 degrees, with both the yaw maneuver data (black circles and purple pluses) and a small portion of regular on-orbit data (squares and triangles).

where there are no regular on-orbit data,; otherwise, we use $\tau_{SD}^{R}\,\mathrm{BRDF}_{\mathrm{RTA}}$ from the regular on-orbit data. Since there are regular on-orbit data on every orbit, the $\tau_{SD}^{R}\,\mathrm{BRDF}_{\mathrm{RTA}}$ from the regular on-orbit data is densely packed along the solar azimuth angular direction, shown in Fig. 7. The high density allows for averaging along the azimuth angular direction to reduce noise. At each φ_V, we carry out a simple average within a window of 0.1 degree.

To obtain $\tau_{SD}\,\mathrm{BRDF}$, we scale the determined $\tau_{SD}^{R}\,\mathrm{BRDF}_{\mathrm{RTA}}$ to match the prelaunch values for each (band, detector) in a least-squares sense. Fig. 8 gives examples of the match in the VIIRS coordinate system[5] for the first detector of bands M1 and M7. Fig. 8 clearly reveals that there are systematic differences between the $\tau_{SD}\,\mathrm{BRDF}$ determined from on-orbit data and measured prelaunch. Along both the ϕ_V and ϕ_H directions, the prelaunch measured $\tau_{SD}\,\mathrm{BRDF}$ varies more than the on-orbit values. Communications with Raytheon indicate that the differences are probably due to errors in the prelaunch measured $\tau_{SD}\,\mathrm{BRDF}$ [18].

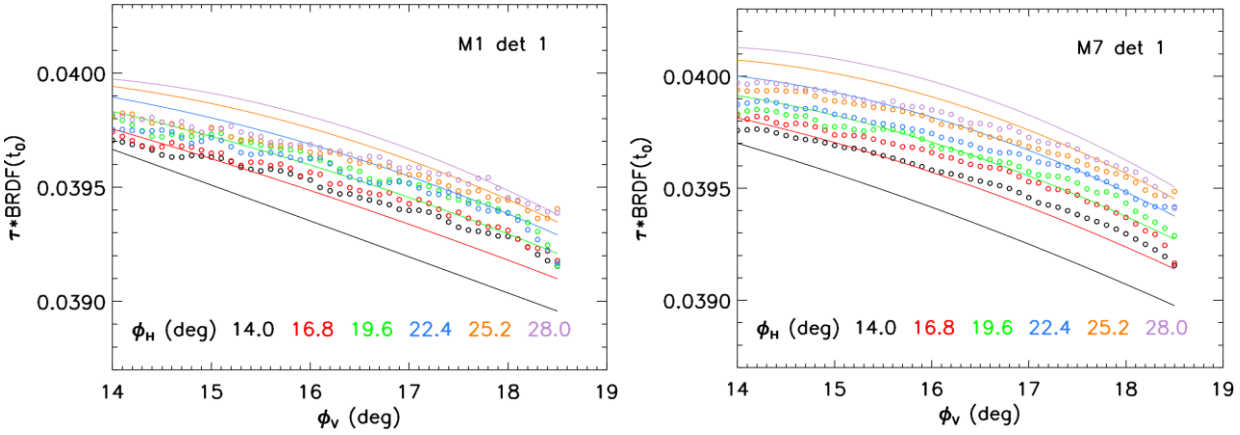

Fig. 8. Calculated $\tau_{SD}^{R}\,\mathrm{BRDF}_{\mathrm{RTA}}$ (circles) scaled to match the prelaunch measured $\tau_{SD}\,\mathrm{BRDF}$ (solid lines) for the first detector of bands M1 and M7.

To validate the $\tau_{SD}\,\mathrm{BRDF}$ calculated with the regular on-orbit data, to reduce the errors in the calculated $\tau_{SD}\,\mathrm{BRDF}$, and to estimate the standard deviation of the errors, we determine $\tau_{SD}\,\mathrm{BRDF}$ again with a different set of regular orbit data (validation data set): orbits centered on 8435 and 6080, from 9217 to 9726, from 9827 to 10080, and from 15984 to 16338. The results from the validation data set are shown as the squares in Fig. 9. The figure shows that the $\tau_{SD}\,\mathrm{BRDF}$ calculated from the original data set and the validation data set behave nearly synchronously, revealing the true $\tau_{SD}\,\mathrm{BRDF}$. Combining the $\tau_{SD}\,\mathrm{BRDF}$ from the two data sets, we estimate the standard deviation of the relative calculation errors to be 0.052%, 0.044%, 0.072%, 0.036%, 0.029%, 0.022%, 0.017%, 0.020%, 0.017%, 0.020%, 0.035%, 0.044%, 0.032%, and 0.046%, for the I1-I3, and M1-M11 bands, respectively.

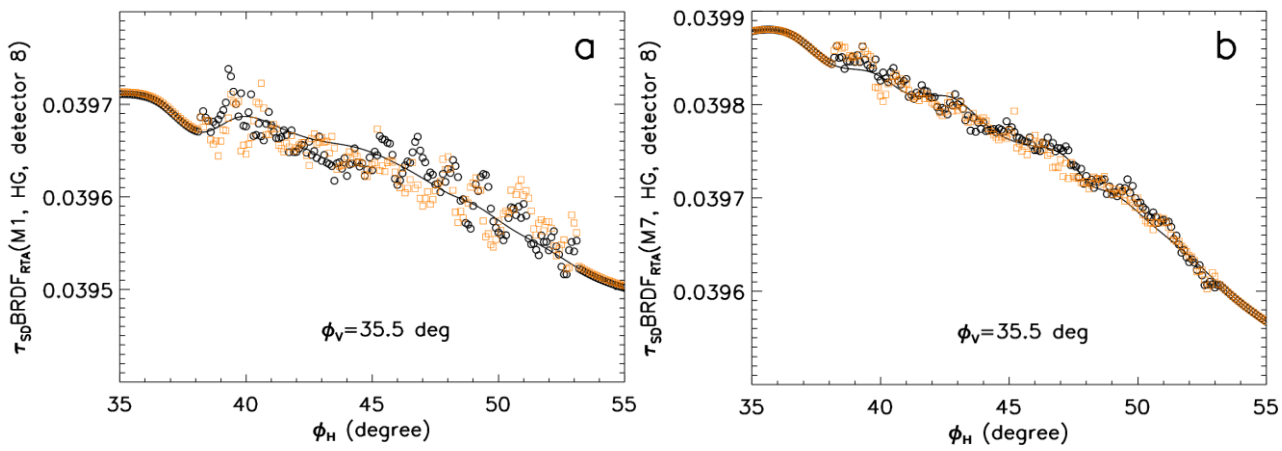

Fig. 8. Calculated τ_{SD} BRDF along ϕ_H at $\phi_V = 35.5°$ from the original data set (circles) and the validation data set (squares) for the 8th detector of band (a) M1 and (b) M7, using SD data in the high-gain stage.

4. SUMMARY

In this study, we have used both the yaw maneuver and a small portion of regular on-orbit data to determine the relative product of the SD screen transmittance and the BRDF at the launch time for the RTA SD view direction. In determining the product, we have removed the bias that existed previously, caused by the angular dependence of the BRDF degradation factor. To reduce the adverse impact of the non-linear drifts in the RSB detector gain and the solar power, we divided the small portion of regular on-orbit data into smaller segments in time. The solar angles of each of the data segment covers those of one yaw maneuver orbit. We calculated the relative product with the yaw maneuver data and each regular on-orbit data segment. We scaled the relative product calculated from the regular on-orbit data segment to match the relative product from the yaw maneuver data. To remove the possible error in the change rate (in time) of the RSB detector gain and the solar spectral power, we used the mismatch in the relative product values at the neighboring segment boundaries. The relative product values at the boundaries should be the same since the data are the same, although assigned to different data segments. To reduce the random noise in the calculated relative product, we used the fact that the solar angles of the regular on-orbit data along the solar azimuth angular direction are densely packed, reflecting the fact that there are sunlit SD data for every satellite orbit. We averaged the product along the solar azimuth angular direction with a 0.1 degree window. To obtain the absolute product of the SD screen transmittance and the BRDF at the launch time for the RTA SD view direction, we scaled the relative product to product measured prelaunch. Systematic differences exist between the products determined from on-orbit data and prelaunch. The prelaunch measured product varies much faster along the solar angles than the product calculated here with the on-orbit data. To determine and reduce the errors in the calculated product, we calculated the product again with a different set of regular on-orbit data. The product determined from the second on-orbit data set behaves nearly synchronously with the one from the first on-orbit data set, validating our results. Averaging the products from the two on-orbit data sets, the standard deviations of the relative errors in the calculated product are estimated to be (not accounting for the systematic error due to errors in the prelaunch measured product): 0.052%, 0.044%,

0.072%, 0.036%, 0.029%, 0.022%, 0.017%, 0.020%, 0.017%, 0.020%, 0.035%, 0.044%, 0.032%, and 0.046%, for the I1-I3, and M1-M11 bands, respectively. We expect that the product determined in this study will improve the precision in the calculated sensor gain change.

ACKNOWLEDGMENT

We would like to thank Kevin Twedt of Science Systems and Applications, Inc. for many useful comments on the manuscript.

REFERENCES

[1] Xiong,X., Sun,J., Barnes,W. and Salomonson,V., "Multiyear on-orbit calibration and performance of Terra MODIS reflective solar bands", *IEEE Trans. Geosci. Remote Sens.,* Vol. 45, 879-889 (2007).

[2] Xiong,X., Sun,J., Xie, X., Barnes, W, and Salomonson, V., "On-Orbit Calibration and Performance of Aqua MODIS Reflective Solar Bands", *IEEE Trans. Geosci. Remote Sens.*, vol. 48, no. 1, pp. 535-546, (2010).

[3] Murphy, R. P., Ardanuy, P. E., De Luccia, F., Clement, J. E. and Schueler, C., "The visible infrared imaging radiometer suite", in *Earth Science Satellite Remote Sensing*,Vol. 1, 199-223, Springer-Verlag: New York, USA (2006).

[4] Cao, C., De Luccia, F. J., Xiong, X., Wolfe, R., and Weng, F., "Early On-Orbit Performance of the Visible Infrared Imaging Radiometer Suite Onboard the Suomi National Polar-Orbiting Partnership(S-NPP) Satellite", *IEEE Trans. Geosci. Remote Sens.*, vol. 52, no. 2, pp. 1142-1156, (2014).

[5] Lei, N., Wang, Z., and Xiong, X., "On-orbit Radiometric Calibration of Suomi NPP VIIRS Reflective Solar Bands through Observations of a Sunlit Solar Diffuser Panel", *IEEE Trans. Geosci. Remote Sens.*, vol. 53, pp. 5983-5990, (2015), DOI: 10.1109/TGRS.2015.2430814.

[6] Xiong, X., Butler, J., Chiang, K., Efremova, B., Fulbright, J., Lei, N., McIntire, J., Oudrari, H., Sun, J., Wang, Z., and Wu, A., "VIIRS On-orbit Calibration Methodology and Performance", *J. of Geo. Res.: Atmosphere*, vol. 119, pp. 5065-5078, (2014).

[7] Joint Polar Satellite System (JPSS) VIIRS Radiometric Calibration Algorithm Theoretical Basis Document (ATBD); NASA Goddard Space Flight Center: Greenbelt, MD, USA, (2013).

[8] Stiegman, A. E., Brinza, D. E., Laue, E. G., Anderson, M. S., and Liang, R. H., "Vacuum Ultraviolet Radiation/Atomic Oxygen Synergism in Fluorinated Ethylene Propylene Teflon Erosion", *J. Spacecraft and Rockets*, vol. 29, pp. 150-151, (1992).

[9] Stiegman, A. E. and Springsteen, A. W., "Ultraviolet stability and contamination analysis of Spectralon diffuse reflectance material", *Opt. Engineering*, vol. 32, pp. 799-804, (1993).

[10] Fulbright, J.,Lei, N., Efremova, B., and Xiong, X., "Suomi-NPP VIIRS Solar Diffuser Stability Monitor Performance", *IEEE Trans. Geosci. Remote Sens.*, vol. 54, pp. 631-639, (2016), DOI: 10.1109/TGRS.2015.2441558.

[11] Xiong, X., Butler, J., Barnes, W., and Guenther, B., "Sensor on-orbit calibration and characterization using spacecraft maneuvers," in *Proc. IEEE Int. Geosci. Remote Sens. Symp.*, 2007, pp. 2256-2259.

[12] Lei, N., Chen, X., and Xiong, X., "Determination of the SNPP VIIRS SDSM screen transmittance from both yaw maneuver and regular on-orbit data", in *Proc. SPIE*, vol. 9218, (2014), Art ID. 9218-03.

[13] Lei, N., Chen, X., and Xiong, X., "Determination of the SNPP VIIRS SDSM Screen Relative Transmittance from Both Yaw Maneuver and Regular On-Orbit Data", *IEEE Trans. Geosci. Remote Sens.*, vol. 54, pp. 1390-1398, (2016), DOI: 10.1109/TGRS.2015.2480039.

[14] Lei, N. and Xiong, X., "Estimation of the Accuracy of the SNPP VIIRS SD BRDF Degradation Factor Determined by the Solar Diffuser Stability Monitor", in *Proc. SPIE*, vol. 9607, (2015), Art ID. 9607-1V.

[15] Lei, N. and Xiong, X., "Impact of the angular dependence of the SNPP VIIRS solar diffuser BRDF degradation factor on the radiometric calibration of the reflective solar bands", in *Proc. SPIE*, vol. 9607, (2015), Art ID. 9607-1Y.

[16] McIntire, J., Moyer, D., Efremova, B., Oudrari, H., and Xiong, X., "On-orbit Characterization of S-NPP VIIRS Transmission Functions", *IEEE Trans. Geosci. Remote Sens.*, vol. 53, pp. 2354-2892, (2015).

[17] Lei, N. and Xiong, X., "Products of the SNPP VIIRS SD Screen Transmittance and the SD BRDFs from Both Yaw Maneuver and Regular On-orbit Data", submitted to *IEEE Trans. Geosci. Remote Sens.*

[18] Private communications with Vijay Murgai of Raytheon.